Vol. 19, e190019 (2022)
doi: 10.2142/biophysico.bppb-v19.0019

Biophysics and Physicobiology
https://www.jstage.jst.go.jp/browse/biophysico/

Regular Article

Structures of oxygen dissociation intermediates of 400 kDa V2 hemoglobin provide coarse snapshots of the protein allostery

Nobutaka Numoto[1], Seiko Onoda[2], Yoshiaki Kawano[3], Hideo Okumura[4], Seiki Baba[4], Yoshihiro Fukumori[5], Kunio Miki[6], Nobutoshi Ito[1]

[1] *Medical Research Institute, Tokyo Medical and Dental University (TMDU), Bunkyo-ku, Tokyo 113-8510, Japan*
[2] *Graduate School of Natural Science and Technology, Kanazawa University, Kanazawa, Ishikawa 920-1192, Japan*
[3] *RIKEN SPring-8 Center, Sayo, Hyogo 679-5148, Japan*
[4] *Structural Biology Division, Japan Synchrotron Radiation Research Institute, Sayo, Hyogo 679-5198, Japan*
[5] *Nano Life Science Institute, Kanazawa University, Kanazawa, Ishikawa 920-1192, Japan*
[6] *Graduate School of Science, Kyoto University, Kyoto 606-8502, Japan*

Received January 24, 2022; Accepted May 9, 2022;
Released online in J-STAGE as advance publication May 12, 2022
Edited by Midori Murakami

Ever since the historic discovery of the cooperative oxygenation of its multiple subunits, hemoglobin (Hb) has been among the most exhaustively studied allosteric proteins. However, the lack of structural information on the intermediates between oxygenated and deoxygenated forms prevents our detailed understanding of the molecular mechanism of its allostery. It has been difficult to prepare crystals of intact oxy-deoxy intermediates and to individually identify the oxygen saturation for each subunit. However, our recent crystallographic studies have demonstrated that giant Hbs from annelids are suitable for overcoming these problems and can provide abundant information on oxy-deoxy intermediate structures. Here, we report the crystal structures of oxy-deoxy intermediates of a 400 kDa Hb (V2Hb) from the annelid *Lamellibrachia satsuma*, following up on a series of previous studies of similar giant Hbs. Four intermediate structures had average oxygen saturations of 78%, 69%, 55%, and 26%, as determined by the occupancy refinement of the bound oxygen based on ambient temperature factors. The structures demonstrate that the cooperative oxygen dissociation is weaker, large ternary and quaternary changes are induced at a later stage of the oxygen dissociation process, and the ternary and quaternary changes are smaller with local perturbations. Nonetheless, the overall structural transition seemed to proceed in the manner of the MWC two-state model. Our crystallographic snapshots of the allosteric transition of V2Hb provide important experimental evidence for a more detailed understanding of the allostery of Hbs by extension of the Monod–Wyman–Changeux (MWC) model.

Key words: oxygenation property, cooperativity, structural change, allosteric effector

Significance

Crystal structures of oxy-deoxy intermediates of 400 kDa giant hemoglobin in intact form provide snapshots of the allosteric transition and strongly support an extension of the MWC model.

Corresponding author: Nobutaka Numoto, Medical Research Institute, Tokyo Medical and Dental University (TMDU), 1-5-45 Yushima Bunkyo-ku, Tokyo 113-8510, Japan. ORCID iD: https://orcid.org/0000-0001-6113-9792, e-mail: numoto.str@mri.tmd.ac.jp

Introduction

The allosteric nature of proteins has been widely studied for over half a century [1,2] as the "second secret of life" [3]; this nature impacts the behavior of protein molecules broadly, affecting metabolism and signaling pathways, and providing clues to drug development. Arguably the most exhaustively studied allosteric protein is hemoglobin (Hb), beginning with the discovery of the Bohr effect [4]. Subsequent milestones of the theoretical Monod−Wyman−Changeux (MWC) model [5] and the stereochemical model based on the crystal structures of oxygenated (oxy) and deoxygenated (deoxy) forms [6] have provided a compelling explanation of the cooperative oxygen-binding mechanism via multiple-subunit molecules. However, only a small amount of intact structural information about intermediates between oxy and deoxy forms [7-9] has been available to date. One of the major reasons for this lack of information is that it remains challenging to prepare crystals of oxy-deoxy intermediates and to identify oxygen saturation individually for each subunit in a crystal.

We have determined the crystal structures of 24-meric giant Hbs from marine annelids [10,11], which show D_3 symmetry with six copies of each of the four subunits (Figure 1A). Recently we reported that bound oxygen of the crystals of the giant Hbs can gradually dissociate thorough the soaking method [11,12], and that the oxygen saturation of each subunit can be determined by the occupancy refinement of the bound oxygen based on ambient temperature factors [12]. In this study, we report the crystal structures of oxy-deoxy intermediates of 400 kDa giant Hb (V2Hb) from the annelid *Lamellibrachia satsuma* by applying the above methods. In comparison to a previous analysis of the intermediate structures of a giant Hb [12] from another species, *Oligobrachia mashikoi* (*Oli*Hb), we reveal significant differences in the allosteric transitions of V2Hb. Correlations of the transition of oxygen saturations in the dimer subassemblies are weaker, the oxygen saturation at which a large structural change occurs is significantly lower, and ternary and quaternary changes are smaller with local perturbations than those observed in *Oli*Hb. Our intermediate structures of V2Hb together with those of *Oli*Hb provide important experimental evidence for understanding the allosteric mechanism of Hb based on extensions of the MWC model.

Materials and Methods

Sample Preparation

The tubeworm *L. satsuma* was collected and the 400 kDa V2Hb was purified as reported previously [11]. Briefly, the blood of the worm was loaded onto a size exclusion column (Sephacryl S-400; Cytiva), and fractions with ratios of absorbance of around 2.8 at 416 nm to 280 nm were collected.

Oxygen Equilibrium Measurements

A Thunberg cuvette cell was connected to a vacuum pump to evacuate the air inside the cell. A mixture of 99.05% helium and 0.95% butane gas was injected into the cell and 3 ml of a 50 μM of V2Hb solution (pH 6.6) was added and shaken slowly for 30 min. The absorption spectrum from 450 nm to 650 nm was measured; then, a small amount of air was injected into the cuvette cell and equilibrated for 15-30 min, followed by the measurement of the absorption spectrum, until the sample reached a fully oxy form. The partial pressure of oxygen at half-saturation (P_{50}) was calculated by the absorption changes at 550 and 570 nm, and cooperativity values (n_{max}) were obtained from the maximum slope of the Hill plot.

Crystallization

The protein was desalted and concentrated to 20-35 mg/ml by ultrafiltration in a solution of 50 mM Tris-HCl pH 7.2 and 10 mM $CaCl_2$ or $MgCl_2$. Bright red crystals were obtained by the sitting-drop vapor diffusion method at 20°C using equal volumes of protein solution and reservoir solution containing 14-17% (w/v) polyethylene glycol (PEG)-3350 and 100 mM HEPES-NaOH pH 7.5. Crystals grew to typical dimensions of 0.3 mm × 0.3 mm × 0.5 mm.

Deoxygenation of the Oxy Crystals

The oxy crystals were soaked in buffer containing 20% (v/v) PEG-400, 18-20% PEG-3350, and 100 mM HEPES-NaOH pH 7.5. The PEG-400 concentration was increased stepwise by 5%, 10%, and 15%, each for 5-10 s. The crystals were then soaked in the final buffer containing 50 mM sodium hydrosulfite, 20% PEG-400, 18-20% PEG-3350, and 100 mM HEPES-NaOH pH 7.5. The dissociation of the bound oxygen is not solely dependent on the concentration of sodium hydrosulfite, it is crucial to increase the concentration of PEG400 at the same time, and increasing the concentration of sodium hydrosulfite alone is insufficient. Since oxygen re-binding were observed in the long soaking, the crystals were incubated for 3-180s. The crystals were immediately flash-frozen under a nitrogen gas stream at -183°C.

Microspectrometry

The absorption spectra of the soaked crystals were measured and corrected for the air blank baseline under a nitrogen-

gas cryostream using an online microspectrophotometer at beamline BL38B1 [13].

Data Collection, Model Building, and Refinement

X-ray diffraction experiments were performed on beamlines BL38B1 and BL41XU at SPring-8, BL-5A at KEK PF, and NW12A at KEK PF-AR. All data were processed and scaled using XDS [14] and truncated by the CCP4 software suite [15]. The structures of V2Hb [PDB ID: 3wct or 3wcu] were used as the search models to determine the initial phases by the molecular replacement method using PHASER [16]. Several cycles of manual model rebuilding and refinement were performed using COOT [17] and PHENIX [18], respectively. No symmetry restraint was applied in the structure refinement though the asymmetric unit contains two copies of each of the four subunits.

Ligand Occupancy Estimation

The occupancies of the bound oxygen molecules at each subunit were estimated as described in our previous study of *Oli*Hb [12]. Briefly, refinements were performed for the oxygen-omitted model; then, oxygen molecules were added to the model, and the XYZ coordinates, atomic displacement parameters (*B*-factors), and group occupancies for the oxygen molecules of each subunit were refined while the parameters for the other atoms remained fixed. The refined occupancies of the oxygen molecules were manually adjusted, and the individual *B*-factors were refined. Iterative occupancy adjustments and *B*-factor refinements of the oxygen molecule were carried out until the refined *B*-factors of the oxygen molecules converged within the standard deviation of the refined *B*-factors of the surrounding atoms (Supplementary Table S1).

The final models were validated by MOLPROBITY [19]. The statistics for data collection and refinement are summarized in Table 1. The figures were prepared using PYMOL software (http://www.pymol.org/).

The atomic coordinates and experimental data (PDB ID: 7vlc, 7vld, 7vle, and 7vlf for the structures of 78%, 69%, 55%, and 26% oxygen saturation, respectively) have been deposited in the Protein Data Bank (www.wwpdb.org).

Results

Oxygenation Properties of V2Hb

Our previous study demonstrated that the crystal structure of V2Hb is quite similar to that of *Oli*Hb, but some local differences such as a lack of inter-subunit disulfide bonds or glycosylation were observed in V2Hb. To address whether the oxygenation properties of V2Hb are significantly different from those of *Oli*Hb [20], we measured the oxygen equilibrium of V2Hb. The Hill plot of the oxygen equilibrium (Figure 1B) clarified that the oxygen affinity (P_{50} = 0.095 mmHg) of V2Hb is remarkably higher than that of *Oli*Hb (maximum 0.19 mmHg), though the cooperativity (n_{max} = 1.4)

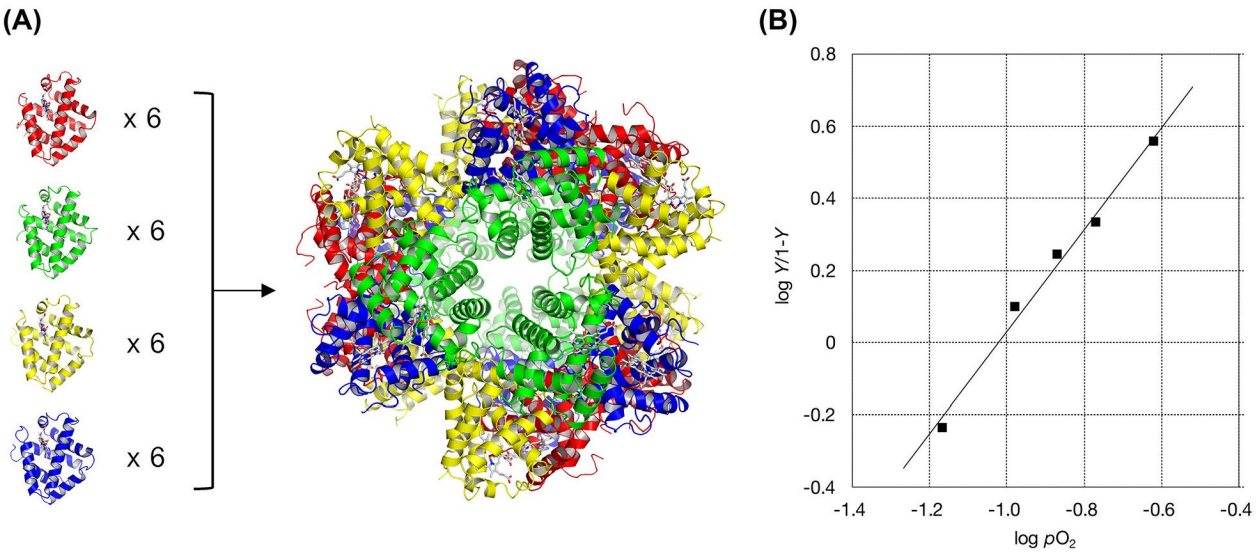

Figure 1 The overall structure and oxygen equilibrium curve of V2Hb. (A) Ribbon diagram of V2Hb. The A1, A2, B1 and B2 subunits are shown in red, green, yellow and blue, respectively. Six copies of each subunit form a spherical 24-mer assembly as a biological unit. (B) Hill plot of oxygen binding by V2Hb. *Y*, fractional saturation of Hb with oxygen; pO_2, partial pressure of oxygen in mmHg. Note that the plot appears to be almost linear shape due to limited range of pO_2. The slope of the black line corresponds to the n_{max} value of 1.4.

is comparable to that of *Oli*Hb in the absence of a divalent cation as an allosteric effector. We have previously reported that the divalent cations would have no contribution to the cooperativity of V2Hb because all cation binding sites are located on the surface of the molecule and no inter-subunit interactions are mediated through the bound ions [11].

Table 1 Data collection and refinement statistics

Data collection	Data 1 (7vlc)	Data 2 (7vld)	Data 3 (7vle)	Data 4 (7vlf)
Soaking time (sec)	20	60	40	90
Wavelength (Å)	1.0000	1.0000	1.0000	1.0000
Space group	$P6_3$	$P6_3$	$P6_3$	$P6_3$
Unit-cell (*a* / *c*) (Å)	109.2 / 194.7	110.3/ 197.0	109.6 / 195.5	109.0 / 194.7
Resolution (Å)	50-2.20 (2.33-2.20)	50-2.10 (2.23-2.10)	50-2.30 (2.44-2.30)	50-2.40 (2.54-2.40)
No. of observations	711,971	784,723	652,863	590,159
No. of unique reflection	66,402	77,995	58,863	51,085
Completeness (%)	99.9 (99.8)	98.9 (93.6)	99.9 (99.5)	99.9 (99.8)
Average $I/\sigma(I)$	17.2 (2.0)	17.8 (1.4)	15.6 (1.8)	23.3 (4.6)
Redundancy	10.7 (7.0)	10.1 (5.3)	11.1 (9.1)	11.6 (11.6)
R_{sym} (%)	8.7 (83.7)	8.8 (105)	12.2 (132)	7.5 (53.5)
$CC_{1/2}$ (%)	99.9 (71.7)	99.9 (52.9)	99.9 (58.4)	99.9 (86.6)
Refinement				
R / R_{free} (%)	19.8 / 24.2	19.0 / 22.1	20.3 / 24.7	24.5 / 27.4
Average *B*-factor (Å^2)	49.4	39.4	44.8	53.0
Number of atoms				
Protein	9,104	9,150	9,112	9,120
Heme and oxygen	360	360	360	352
Carbohydrate	48	48	48	48
Ca^{2+}	2	2		2
Water	427	798	316	113
RMSD from ideal				
Bonds (Å)	0.004	0.003	0.005	0.003
Angles (°)	0.60	0.61	0.75	0.60
Ramachandran plot				
Favored region (%)	98.10	98.53	97.80	97.67
Allowed region (%)	1.90	1.30	2.20	2.25
Outlier region (%)	0	0.17	0	0.09

Values for the outer shell are given in parentheses.

Oxygen Dissociation in Crystalline V2Hb

Our previous study demonstrated that the oxy crystal of V2Hb can shift to the deoxy form, and a crystalline state could be maintained by soaking in a solution containing 50 mM sodium hydrosulfite [11]. To obtain crystals of the oxy-deoxy intermediate state, we tested various soaking times from 3 s to 180 s and then immediately flash-froze the crystals under a nitrogen gas stream at 95 K. The oxygenation state of the crystals was verified by the absorption spectra (Figure 2) of the crystals using an online microspectrophotometer at beamline BL38B1 of SPring-8 [13]. Thin platelike crystals of about 50 μm or less were used to avoid signal saturation. The spectra from the 20 s and 60 s soakings clearly showed patterns that were intermediate between the typical spectra from the oxy and deoxy Hb. These facts demonstrate that the soaking method described above is useful to obtain oxy-deoxy intermediate crystals. The spectra also indicated that the

crystal from the 20 s soaking is closer to the deoxy state than the crystal from the 60 s soaking. While this may appear to be contradictory, in fact it would be attributable to the difference in crystal thickness, because a longer soaking time would be required for thicker crystals to achieve sufficient oxygen dissociation. It was so difficult to prepare crystals of precisely consistent thickness because at the time we collected the data, crystal processing machines [21] were not yet available. This made it difficult to control the oxygen saturation rate by soaking time alone. Moreover, thin crystals of less than 50 μm gave only low-resolution diffraction in spite of the experiments at the synchrotron facilities. Therefore, we finally employed thick, large crystals of more than 100 μm and prepare kinds of crystals with various soaking times to collect X-ray diffraction data for a variety of oxygen saturation levels. And we decided to estimate the oxygen saturation (i.e. occupancy) by structural refinement using the previously reported method [12] based on ambient temperature factors.

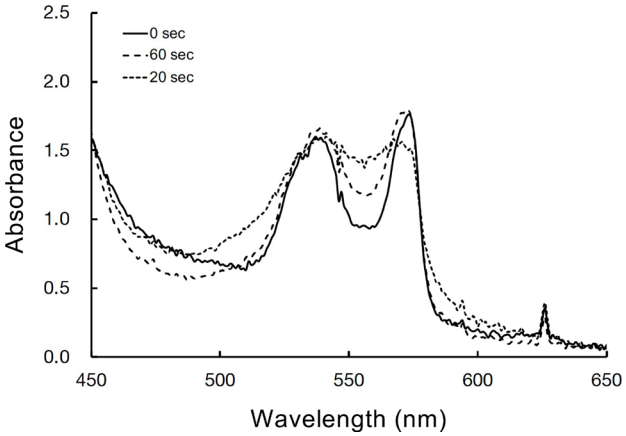

Figure 2 Absorption spectra of the oxy-deoxy intermediate crystals of V2Hb. Data were measured using thin platelike crystals independently of the diffraction experiments via microspectrophotometer. The soaking times are shown in the inset of the diagram. The peaks around 630 nm are derived from the emission lines of the Hg–Xe lamp.

Oxygen Dissociation at Each Heme Pocket

Ample X-ray diffraction data were collected for various soaking times and obtained four identical intermediate structures (designated as Data 1, 2, 3, and 4) determined at 2.2, 2.1, 2.3, and 2.4 Å resolution, respectively. As reported previously, the 24meric whole V2Hb molecule shows D_3 symmetry with six copies of each of the four subunits [11]. The crystals maintained their packing during soaking, so that they belonged to the same space group of $P6_3$. The asymmetric unit contains two copies of each of the four subunits (A1, A2, B1, B2, A1', A2', B1', and B2'), because the crystallographic three-fold symmetry axis is along the molecular symmetric axis. Significant changes were seen in the electron densities at the heme pockets of each subunit. Roughly, a longer soaking time resulted in weaker electron density at all heme pockets, and the electron density disappeared at 90 s of soaking (Figure 3A).

To determine the quantitative oxygen saturation at each subunit, we refined the coarse occupancy of the bound oxygen based on ambient temperature factors, as reported previously [12]. Supplementary Table S1 shows the refined *B*-factors of the heme-surrounding atoms (Figure 3B) and the estimated occupancy of each oxygen molecule (summarized in Figure 3C). The average occupancy of each subunit provides total oxygen saturation in the crystals of 78%, 69%, 55%, and 26% for Data 1, 2, 3, and 4, respectively. We previously reported that X-ray radiation reduces oxygen saturation by 1-7 percentage points after data collection, when oxygen saturation is 20% or higher [12].

Although V2Hb forms a quaternary assembly identical to that of *Oli*Hb, the observed changes in the occupancy in each subunit suggest more complex correlations among the subunits. The A1 and B1 subunits form a dimer subassembly in the 24meric whole structure, and the A2 and B2 subunits form another dimer. However, there seems to be only moderate correlation between the A1 and B1 subunits or the A2 and B2 subunits, whereas strong correlations are observed in the case of *Oli*Hb [12]. This is also the case for A1' and B1', but there seems to be little correlation between the A2' and B2' subunits. These observations strongly suggested that V2Hb and *Oli*Hb have different cooperativity mechanisms in their structural transitions.

Ternary and Quaternary Structural Changes

We have reported that the most remarkable ternary structural change that directly affects oxygen affinity at the heme pocket is the protrusion of Val E11 towards the heme pocket in giant Hbs [22]. In addition, we have elucidated that the change at the Val E11 is a single-step transition, as suggested in the MWC two-state model by the structural analysis of the oxy-deoxy intermediates of *Oli*Hb [12]. Transitions of the distances between the Cβ atom of Val E11 and the iron of the heme in V2Hb (Figure 4A) clearly confirm similar single-step transitions between Data 3 (55% oxy) and Data 4 (26% oxy). Changes in distances are relatively small to discuss by current resolution, but the feature that Data 4 shows the minimum distance is exactly the same for all eight subunits. This fact will indicate that the protrusion of Val E11 occur between Data 3 and 4, though slight perturbations are observed among Data 1, 2, and 3 (78%-55% oxy). Thus, no significant protrusions of Val E11 occurred even at 55% oxygen saturation, and this is in contrast to the fact that the conformational change at Val E11 of *Oli*Hb is complete at an equivalent (58%) oxygen saturation. Another remarkable ternary structural change was observed at the AB loop region in each subunit. Structural changes of the AB loops of all

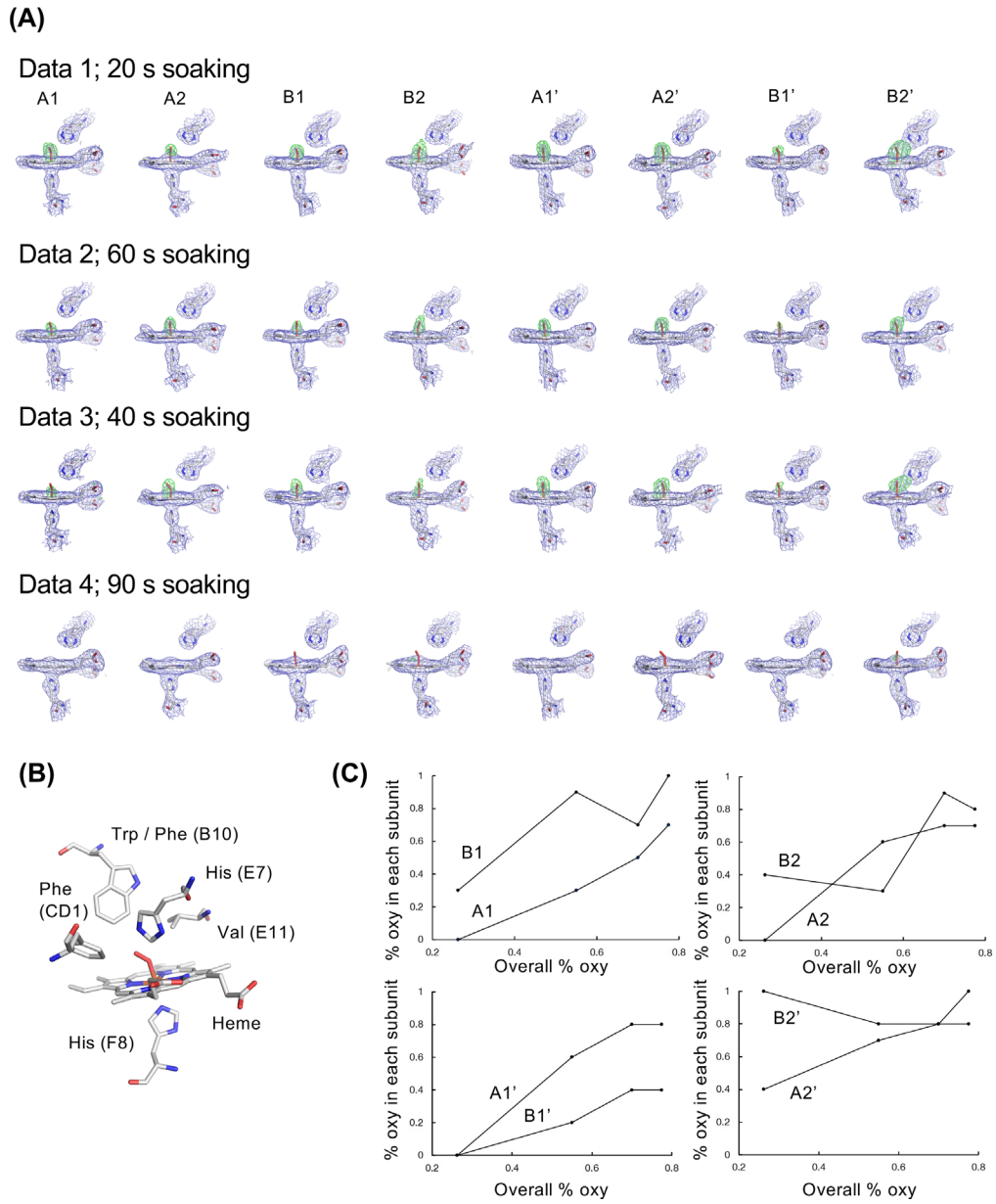

Figure 3 Determination of the oxygen saturation fraction of each subunit. (A) Electron densities superposed on the ligand sites of each subunit. The $2F_o$-F_c maps (blue, contoured at 1.0σ) and the oxygen-omitted F_o-F_c maps (green, contoured at 3.0σ) are represented with stick models of the heme, oxygen, proximal histidine and distal histidine. (B) The residues to which the atoms subjected to the *B*-factor analysis belong are shown as stick models. (C) Transition of oxygen saturation in each subunit (vertical axis). The overall oxygen saturation of the crystals (horizontal axis) was calculated as the average of that of each subunit. Subunits forming the dimer subassembly are shown as a pair in each graph.

subunits are observed when the oxygen saturation falls below 55% (Figure 4B), consistent with the changes at Val E11. These facts indicate that V2Hb undergoes structural changes according to the MWC model as shown in *Oli*Hb, but switching between the R- and T-states (structures of the high and low oxygen affinity, respectively) occurs at lower oxygen saturations. There have been reported a lot of experimental evidence that the changes in the position of iron atoms in heme and distortion of the planar structure of heme between the R-and T-states. However, the resolutions of our structures are still not sufficient to discuss such minute structural changes.

The quaternary structures observed in this study demonstrate that those of Data 1, 2, and 3 (78%, 69%, and 55% oxy, respectively) globally belong to that of the R-state while only the structure of Data 4 (26% oxy) belongs to the T-state.

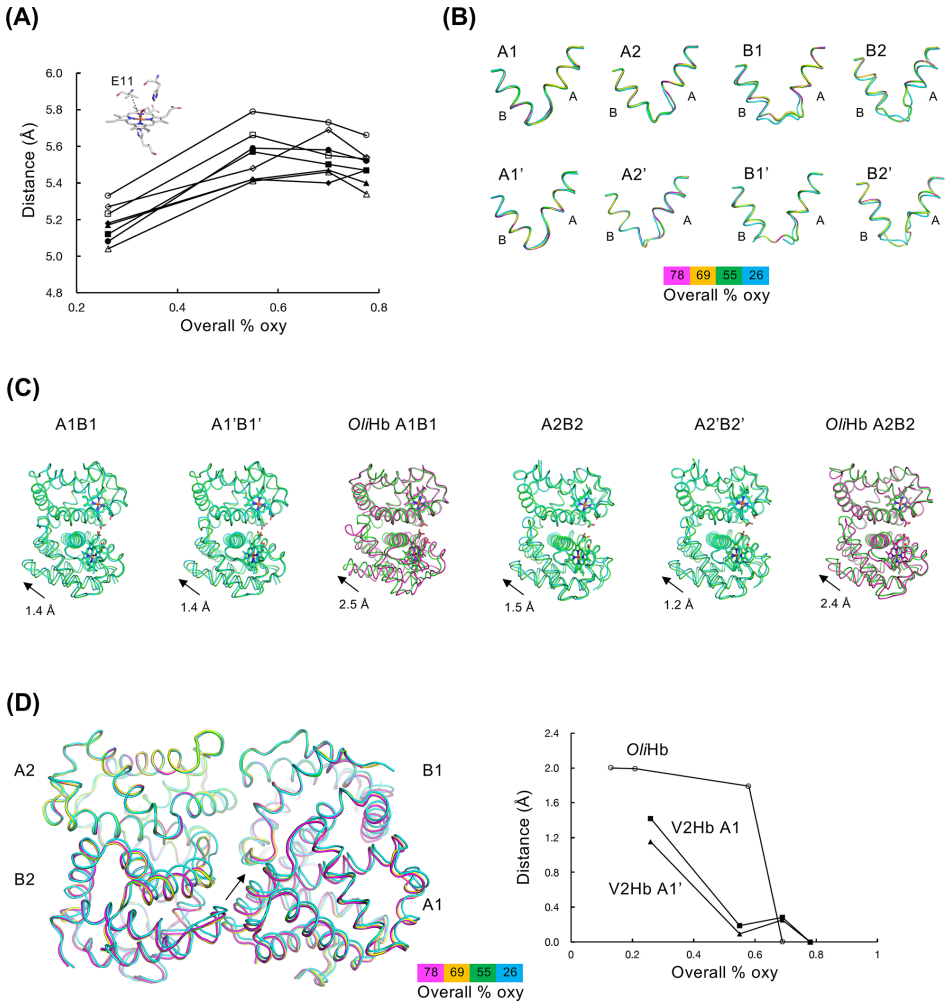

Figure 4 Ternary and quaternary structural transitions of V2Hb. (A) Changes of the distance between the Cβ atom of Val E11 and the iron of the heme (dashed line in the inset) for each subunit. Black circle, A1; black square, A2; black triangle, B1; black rhombus, B2; white circle, A1'; white square, A2'; white triangle, B1'; white rhombus, B2'. (B) Closeup views of the superpositions of the AB loops. Data 1, 2, 3, and 4 are drawn in magenta, yellow, green, and cyan, respectively. The A and B helices are labeled. (C) Quaternary changes of the dimer subassemblies. Superpositions of Data 3 (green) and 4 (cyan) of V2Hb of each dimer subassembly were calculated by only one subunit (upper subunit in the figures) to emphasize the quaternary changes. For comparison, the same superposition was performed for the dimer subassembly of *Oli*Hb (magenta, R-state; green, T-state). Distances at the GH loop (black arrows) are indicated. (D) Quaternary changes of the A1A2B1B2 tetramer subassemblies. The superposition was calculated by only the A2 subunit. The color schemes are the same as in panel B. The transition of the A helix of the A1 subunit (black arrow) was evaluated by the distances at the Cα atoms of Met12 between Data 1 and 2, 3, and 4, respectively, and plotted in the right panel. For comparison, the same calculations were performed for the A1'A2'B1'B2' tetramer of V2Hb and the same tetramer of *Oli*Hb. Black square, transition of A1 of V2Hb; black triangle, transition of A1' of V2Hb; white circle, transition of A1 of *Oli*Hb. All superpositions were calculated by an "align" command of program PyMOL (http://www.pymol.org/), in which a superposition is performed by utilizing the sequence alignment information and rejecting structural outlier atoms.

This is in good agreement with the observed ternary changes, suggesting that the ternary and quaternary changes are well synchronized. We have previously reported the mechanism of the heme-heme communication in the giant Hb [23]. The propionic acid of the heme directly interacts with the side chain of Arg/His F3 and Gln F7 of the adjacent subunit of EF-dimer, thus the structural change of one heme directly transmits to the adjacent F helix that bound the other heme.

However, quaternary changes in the dimer subassemblies show that the relative changes between the A1 and B1 subunits and also between the A2 and B2 subunits are smaller than those of *Oli*Hb (Figure 4C). These facts would explain, at least in part, why the oxygen dissociation of each subunit of V2Hb has a weaker correlation between dimer subassemblies than those of *Oli*Hb. Analysis of the relative movement of the A1 (A1') subunit in the tetramer subassembly in the

superposition of the A2 (A2') subunit, which indicates a large quaternary rearrangement beyond the dimer subassembly, also shows a single-step transition, though the changes are smaller than those observed in *Oli*Hb (Figure 4D). Thus, the quaternary changes at both the dimer and tetramer subassemblies are well-correlated but smaller than those of *Oli*Hb. Smaller ternary changes at the AB loops would cause such relatively small quaternary changes.

Discussion

In this study, we determined four intermediates of the allosteric transition of V2Hb and produced coarse snapshots of giant hemoglobin that differ from those of *Oli*Hb previously reported [12]. As the P_{50} value of V2Hb reported here is significantly higher than that of *Oli*Hb [20], it seems likely that the allosteric transitions of these two giant Hbs proceed in significantly different manners. The intermediate structures of both V2Hb in this study and *Oli*Hb provide a useful basis for discussing in detail the molecular mechanism underlying the allostery of Hbs.

The higher oxygen affinity of V2Hb is confirmed by our intermediate structures, which demonstrate that the structures maintain the R-state up to overall 55% oxy, even though the oxygen occupancies of the A1, B2, and B1' subunits are significantly lower than 0.5. The R-state of V2Hb will be stable without inter-subunit divalent cations, whereas *Oli*Hb requires divalent cations bound to the interface of the subunits to stabilize the R-state [20,23].

The transition of the oxygen saturation of each subunit revealed that the correlations between the subunits in the dimer subassemblies of V2Hb are weaker than those observed in *Oli*Hb. Thus, the quaternary changes at the interfaces of the dimer subassemblies would have little effect on the allosteric oxygen dissociation. A possible explanation of the allosteric mechanism is that the structural change in the AB loop is weakly transmitted into the tetramer subassembly. This hypothesis is supported by the fact that the AB loops and the adjacent A- and B-helices of each of the four subunits are in contact with each other in the tetramer subassembly, and the rearrangements of the bulky sidechains at the AB loops mediate the conformational changes of the E helices, causing the protrusion of Val E11, which is responsible for the oxygen affinity [11].

Diagrams of the transition of the oxygen saturation of A1, A2, B1, and B2, which together form a tetrameric subassembly, are different from those of A1', A2', B1', and B2', which form a different tetrameric subassembly (Figure 3C), despite the fact that these two tetrameric subassemblies are equivalent to each other in the 24meric D_3 symmetry of V2Hb. The lack of the inter-subunit Ca^{2+} ions binding between A1 and A1' may cause unrestrained behavior of the tetramer subassemblies because the two symmetrically equivalent Ca^{2+} ions have been shown to ensure a quaternary change that maintains rotational symmetry between the two tetramers [23].

The ternary and quaternary structural changes in V2Hb seem to follow the MWC two-state model, even with some local perturbations. It should be noted that electron densities clearly demonstrate that the simultaneous mixture of the structures of the R- and T-states in a crystal is not observed at all in V2Hb or *Oli*Hb. That is, we found few data to support the KNF sequential model [24], which is the alternative authentic model to explain the allostery of Hbs by independent conformational change of each subunit (i.e. multi-step transitions).

Extended MWC models have been proposed by Yonetani *et al.* [25-27], and Shibayama *et al.* [28]. The results of our crystallographic studies could be understood without any conflict using these models. Yonetani *et al.* showed that even if the structural transition between the R- and T-states is the same, the oxygen affinity and cooperativity can vary enormously depending on the allosteric effectors, and on whether and how much the effectors stabilize the R- and T-states. The significant difference in oxygen affinity between V2Hb and *Oli*Hb that is supported by the intermediate structure analyses can be interpreted as the contribution of the allosteric effector of divalent cations. A series of studies of human Hb by Shibayama *et al.* [29-31] have revealed a large number of structural variants of both the R- and T-states. Local perturbations such as the protrusion of Val E11 or the quaternary structures of the tetramer subassembly observed in our intermediate structures of V2Hb can be considered as structural variations within the R-state. Therefore, the results of our analysis of V2Hb intermediate structures are consistent with the above results clarified mainly by analyses of human Hb.

Conclusion

We measured the oxygenation properties of V2Hb and demonstrated that remarkably higher oxygen affinity and comparable cooperativity with those of *Oli*Hb, which is the same 24 meric giant Hb. We determined four oxygen dissociation intermediate structures of V2Hb. Average oxygen saturations of 78%, 69%, 55%, and 26% were determined by the occupancy refinement of the bound oxygen based on ambient temperature factors. The higher oxygen affinity of V2Hb is confirmed by the fact that large ternary and quaternary structural changes occur in the latter stage of the oxygen dissociation process. Our snapshots of the allosteric transitions of two giant Hbs, V2Hb and *Oli*Hb, thus provide crucial experimental evidence that the allosteric mechanism can be understood by the extensions of the MWC model.

Conflict of Interest

The authors declare no competing financial interest.

Author Contributions

N.N., Y.F., K.M., and N.I. designed the work. N.N. performed the structure analyses. S.O. performed the oxygen equilibrium measurements. N.N., Y.K., H.O., and S.B. performed microspectrometric analyses. N.N. drafted the paper and figures. All authors revised the manuscript.

Acknowledgements

This work was supported by JSPS KAKENHI Grants (Nos. 25870200 and 15K20971) to N.N. X-ray crystal structure analyses were performed with the approval of the Japan Synchrotron Radiation Research Institute (Proposal No. 2014A1159) and the Photon Factory Program Advisory Committee (Proposal Nos. 2013G126 and 2013G623).

References

[1] Fenton, A. W. Allostery: An illustrated definition for the 'second secret of life'. Trends Biochem. Sci. 33, 420-425 (2008). https://doi.org/10.1016/j.tibs.2008.05.009

[2] Liu, J., Nussinov, R. Allostery: An overview of its history, concepts, methods, and applications. Plos Comput. Biol. 12, e1004966 (2016). https://doi.org/10.1371/journal.pcbi.1004966

[3] Monod, J. On chance and necessity in studies in the philosophy of biology: Reduction and related problems (Ayala, F. J., Dobzhansky, T. eds) pp. 357-375 (Macmillan Education UK, London, 1974). https://doi.org/10.1007/978-1-349-01892-5_20

[4] Bohr, C., Hasselbach, K. A., Krogh, A. Über einen in biologischen beziehung wichtigen einfluss, den die kohlen-sauerspannung des blutes auf dessen sauerstoffbindung übt. Skand. Arch. Physiol. 15, 401-412 (1904).

[5] Monod, J., Wyman, J., Changeux, J. P. On the nature of allosteric transitions: A plausible model. J. Mol. Biol. 12, 88-118 (1965). https://doi.org/10.1016/s0022-2836(65)80285-6

[6] Perutz, M. F. Stereochemistry of cooperative effects in haemoglobin. Nature 228, 726-734 (1970). https://doi.org/10.1038/228726a0

[7] Knapp, J. E., Pahl, R., Cohen, J., Nichols, J. C., Schulten, K., Gibson, Q. H., et al. Ligand migration and cavities within *Scapharca* dimeric HbI: Studies by time-resolved crystallo-graphy, xe binding, and computational analysis. Structure 17, 1494-1504 (2009). https://doi.org/10.1016/j.str.2009.09.004

[8] Knapp, J. E., Pahl, R., Srajer, V., Royer, W. E., Jr. Allosteric action in real time: Time-resolved crystallographic studies of a cooperative dimeric hemoglobin. Proc. Natl. Acad. Sci. U.S.A. 103, 7649-7654 (2006). https://doi.org/10.1073/pnas.0509411103

[9] Nienhaus, K., Knapp, J. E., Palladino, P., Royer, W. E., Jr., Nienhaus, G. U. Ligand migration and binding in the dimeric hemoglobin of *Scapharca inaequivalvis*. Biochemistry 46, 14018-14031 (2007). https://doi.org/10.1021/bi7016798

[10] Numoto, N., Nakagawa, T., Kita, A., Sasayama, Y., Fukumori, Y., Miki, K. Structure of an extracellular giant hemoglobin of the gutless beard worm *Oligobrachia mashikoi*. Proc. Natl. Acad. Sci. U.S.A. 102, 14521-14526 (2005). https://doi.org/10.1073/pnas.0501541102

[11] Numoto, N., Nakagawa, T., Ohara, R., Hasegawa, T., Kita, A., Yoshida, T., et al. The structure of a deoxygenated 400 kDa haemoglobin reveals ternary- and quaternary-structural changes of giant haemoglobins. Acta Crystallogr. D Biol. Crystallogr. 70, 1823-1831 (2014). https://doi.org/10.1107/S1399004714008475

[12] Numoto, N., Kawano, Y., Okumura, H., Baba, S., Fukumori, Y., Miki, K., et al. Coarse snapshots of oxygen-dissociation intermediates of a giant hemoglobin elucidated by determining the oxygen saturation in individual subunits in the crystalline state. IUCrJ 8, 954-962 (2021). https://doi.org/10.1107/S2052252521009386

[13] Shimizu, N., Shimizu, T., Baba, S., Hasegawa, K., Yamamoto, M., Kumasaka, T. Development of an online UV-visible microspectrophotometer for a macromolecular crystallography beamline. J. Synchrotron Rad. 20, 948-952 (2013). https://doi.org/10.1107/S0909049513022887

[14] Kabsch, W. XDS. Acta Crystallogr. D Biol. Crystallogr. 66, 125-132 (2010). https://doi.org/10.1107/S0907444909047337

[15] Winn, M. D., Ballard, C. C., Cowtan, K. D., Dodson, E. J., Emsley, P., Evans, P. R., et al. Overview of the *CCP*4 suite and current developments. Acta Crystallogr. D Biol. Crystallogr. 67, 235-242 (2011). https://doi.org/10.1107/S0907444910045749

[16] McCoy, A. J., Grosse-Kunstleve, R. W., Adams, P. D., Winn, M. D., Storoni, L. C., Read, R. J. Phaser crystallographic software. J. Appl. Cryst. 40, 658-674 (2007). https://doi.org/10.1107/S0021889807021206
[17] Emsley, P., Lohkamp, B., Scott, W. G., Cowtan, K. Features and development of Coot. Acta Crystallogr. D Biol. Crystallogr. 66, 486-501 (2010). https://doi.org/10.1107/S0907444910007493
[18] Adams, P. D., Afonine, P. V., Bunkoczi, G., Chen, V. B., Davis, I. W., Echols, N., et al. *PHENIX*: A comprehensive python-based system for macromolecular structure solution. Acta Crystallogr. D Biol. Crystallogr. 66, 213-221 (2010). https://doi.org/10.1107/S0907444909052925
[19] Chen, V. B., Arendall, W. B., 3rd, Headd, J. J., Keedy, D. A., Immormino, R. M., Kapral, G. J., et al. *MolProbity*: All-atom structure validation for macromolecular crystallography. Acta Crystallogr. D Biol. Crystallogr. 66, 12-21 (2010). https://doi.org/10.1107/S0907444909042073
[20] Aki, Y., Nakagawa, T., Nagai, M., Sasayama, Y., Fukumori, Y., Imai, K. Oxygenation properties of extracellular giant hemoglobin from *Oligobrachia mashikoi*. Biochem. Biophys. Res. Commun. 360, 673-678 (2007). https://doi.org/10.1016/j.bbrc.2007.06.111
[21] Basu, S., Olieric, V., Leonarski, F., Matsugaki, N., Kawano, Y., Takashi, T., et al. Long-wavelength native-SAD phasing: Opportunities and challenges. IUCrJ 6, 373-386 (2019). https://doi.org/10.1107/S2052252519002756
[22] Numoto, N., Nakagawa, T., Kita, A., Sasayama, Y., Fukumori, Y., Miki, K. Structure of the partially unliganded met state of 400 kDa hemoglobin: Insights into ligand-induced structural changes of giant hemoglobins. Proteins 73, 113-125 (2008). https://doi.org/10.1002/prot.22040
[23] Numoto, N., Nakagawa, T., Kita, A., Sasayama, Y., Fukumori, Y., Miki, K. Structural basis for the heterotropic and homotropic interactions of invertebrate giant hemoglobin. Biochemistry 47, 11231-11238 (2008). https://doi.org/10.1021/bi8012609
[24] Koshland, D. E., Nemethy, G., Filmer, D. Comparison of experimental binding data and theoretical models in proteins containing subunits. Biochemistry 5, 365-385 (1966). https://doi.org/10.1021/bi00865a047
[25] Yonetani, T., Laberge, M. Protein dynamics explain the allosteric behaviors of hemoglobin. Biochim. Biophys. Acta. 1784, 1146-1158 (2008). https://doi.org/10.1016/j.bbapap.2008.04.025
[26] Yonetani, T., Park, S. I., Tsuneshige, A., Imai, K., Kanaori, K. Global allostery model of hemoglobin. Modulation of O_2 affinity, cooperativity, and Bohr effect by heterotropic allosteric effectors. J. Biol. Chem. 277, 34508-34520 (2002). https://doi.org/10.1074/jbc.M203135200
[27] Yonetani, T., Tsuneshige, A. The global allostery model of hemoglobin: An allosteric mechanism involving homotropic and heterotropic interactions. C. R. Biol. 326, 523-532 (2003). https://doi.org/10.1016/s1631-0691(03)00150-1
[28] Shibayama, N. Allosteric transitions in hemoglobin revisited. Biochim. Biophys. Acta. Gen. Subj. 1864, 129335 (2020). https://doi.org/10.1016/j.bbagen.2019.03.021
[29] Shibayama, N., Ohki, M., Tame, J. R. H., Park, S. Y. Direct observation of conformational population shifts in crystalline human hemoglobin. J. Biol. Chem. 292, 18258-18269 (2017). https://doi.org/10.1074/jbc.M117.781146
[30] Shibayama, N., Sato-Tomita, A., Ohki, M., Ichiyanagi, K., Park, S. Y. Direct observation of ligand migration within human hemoglobin at work. Proc. Natl. Acad. Sci. U.S.A. 117, 4741-4748 (2020). https://doi.org/10.1073/pnas.1913663117
[31] Shibayama, N., Sugiyama, K., Tame, J. R. H., Park, S. Y. Capturing the hemoglobin allosteric transition in a single crystal form. J. Am. Chem. Soc. 136, 5097-5105 (2014). https://doi.org/10.1021/ja500380e